CHAPTER 31

Nonconforming Mortar Element Methods: Application to Spectral Discretizations

Yvon Maday*†
Cathy Mavriplis†
Anthony T. Patera†

ABSTRACT

Spectral element methods are p-type weighted residual techniques for partial differential equations that combine the generality of finite element methods with the accuracy of spectral methods. We present here a new ***nonconforming*** discretization which greatly improves the flexibility of the spectral element approach as regards automatic mesh generation and non-propagating local mesh refinement. The method is based on the introduction of an auxiliary "mortar" trace space, and constitutes a new approach to discretization-driven domain decomposition characterized by a clean decoupling of the local, structure-preserving residual evaluations and the transmission of boundary and continuity conditions. The flexibility of the mortar method is illustrated by several nonconforming adaptive Navier-Stokes calculations in complex geometry.

* Laboratoire d'Analyse Numerique de l'Universite Pierre et Marie Curie, Paris, France

† Department of Mechanical Engineering, Massachusetts Institute of Technology, Cambridge, Massachusetts 02139

1 Introduction

Spectral element methods [22,25,27] are weighted residual techniques for the approximation of partial differential equations that combine the rapid convergence rate of spectral methods [6,14] with the generality of finite element techniques [8,12,29]. The spectral element discretization, coupled to fast order-independent iterative solvers [21,28,32], yields numerical algorithms which have proven computationally efficient on both serial and parallel processors [11,10]. Although the spectral element method is, by construction, applicable in complex geometries [16,18,27], the large indestructible geometric unit associated with high-order brick elements leads to a certain lack of flexibility as regards automatic mesh generation, adaptive mesh refinement, and the treatment of moving boundaries. In this paper we present a new method, the "mortar element method", which largely eliminates this rigidity by allowing for nonconforming matching between subdomains.

The "mortar element method" represents a new domain decomposition approach [7,13] in which there is a clean decoupling of local-structure-preserving internal residual evaluations and the transmissions of boundary (or continuity) conditions. The method is not based on Lagrange-multiplier interface constraints e.g. [9], but rather on the explicit construction of the appropriate nonconforming space of approximation through the introduction of a new intermediary mortar trace space. The explicit-space approach is more appropriate for fast iterative solution than the Lagrange-multiplier methods, as it avoids the necessity of solving a coupled, potentially ill-conditioned problem. Although we develop the mortar methods here for spectral element discretizations, they are also

appropriate in the h-type finite element context [4], in which they constitute an extension and generalization of classical nonconforming methods [8,9,29,31].

We present here the "mortar element method" in its simplest form for the solution of two-dimensional second-order elliptic and saddle problems. The emphasis is on the numerical formulation, implementation, and demonstration of the technique, and the illustration of the flexibility of the nonconforming paradigm; theoretical support for the method is given in [4], in which the optimality of the discretization is proven. The outline of the paper is as follows. In Section 2 we present the basic discretization for the Poisson equation in terms of the function spaces over which the standard variational form is to be tested. In Section 3 we present the associated nonconforming bases and the resulting set of discrete equations. Conjugate gradient iterative solution of the mortar discretization is described, illustrating the strong domain decomposition nature of the residual evaluation procedure. In Section 4 the extension of the method to the solution of the Stokes and Navier-Stokes problem is presented. Lastly, in Section 5 we give several numerical examples.

2 Spectral Element Nonconforming "Mortar" Spaces

2.1 Problem Formulation

We consider first the solution of a Poisson equation on a domain Ω of $\mathbf{R}^2$: Find $u(x,y)$ such that

$$-\nabla^2 u = f \quad \text{in } \Omega, \tag{1a}$$

$$u = 0 \quad \text{on } \partial\Omega, \tag{1b}$$

where $\partial\Omega$ is the boundary of Ω, and f is the prescribed force. We suppose that Ω is rectangularly decomposable, that is, that there exist rectangular subdomains Ω^k, $k = 1, ..., K$ such that

$$\overline{\Omega} = \bigcup_{k=1}^{K} \overline{\Omega}^k, \quad \forall k, l,\ k \neq l,\ \Omega^k \cap \Omega^l = \emptyset. \tag{2}$$

The problem (1a,1b) is well posed in $X = H_o^1$ in the sense that the following weak formulation of the problem admits only one solution: Find $u \in X$ such that

$$(\nabla u, \nabla v) = < f, v >, \quad \forall v \in X. \tag{3}$$

Here $(.,.)$ represents the L^2 inner product, and $< .,. >$ denotes the duality pairing between X and its dual space. For the definition of standard spaces, norms and inner products we refer the reader to [1].

For the Galerkin numerical approximation of problem (1a,1b), we test the variational form (3) with respect to a family of discrete finite dimensional spaces X_h, where h denotes a discretization parameter: Find $u_h \in X_h$ such that

$$(\nabla u_h, \nabla v_h) = < f, v_h >, \quad \forall v_h \in X_h. \tag{4}$$

In the case of a conforming approximation, for which $X_h \subset X$, the convergence and convergence rate of u_h towards u is determined essentially by stability (ellipticity and continuity) and approximation theory (infimum of $\|u - v_h\|_{1,\Omega}$ over all $v_h \in X_h$, where $\|\cdot\|_{1,\Omega}$ refers to the H^1 norm over Ω). In the case of nonconforming approximations, for which $X_h \not\subset X$, we must also consider the consistency error, which measures the deviation of the approximation space X_h from the proper space X [8,29].

To date, spectral element approximations [22] have been based on domain decompositions that satisfy (2) as well as the additional constraint that the intersection of two adjacent elements is either an entire edge or a vertex; this second constraint is derived from the conforming assumption,

and is also present in the finite element method. In the spectral element context this constraint can be prohibitively restrictive due to the large geometric units involved. Although relaxing the conforming constraint clearly introduces a new source of error, it has the potential advantage of greatly increasing the flexibility of the numerical method as regards mesh generation and adaptive refinement procedures. This increase in flexibility improves not only the efficiency of the algorithm, but also the tractability of calculations involving moving and sliding meshes [15]. Furthermore, the nonconforming approach achieves generality at no cost in loss of local structure, an important consideration as regards optimal solvers.

We present here a spectral method based on nonconforming approximations in which the consistency errors are commensurate with the approximation errors. To present the nonconforming spectral element space X_h we first describe the anatomy of the discretization. The K rectangular subdomains of (2) are now identified as spectral elements, and the (x, y) coordinate system is chosen so as to be aligned with the edges of the Ω^k. These edges are denoted $\Gamma^{k,l}$, $l = 1, ..., 4$, such that $\partial\Omega^k = \bigcup_{l=1}^{4} \overline{\Gamma}^{k,l}$. We next introduce the set of "mortars" γ^p, where

$$\gamma^p = \text{int}(\overline{\Omega}^k \cap \overline{\Omega}^l) \tag{5a}$$

for some k and l, or

$$\gamma^p = \text{int}(\overline{\Omega}^m \cap \partial\overline{\Omega}) \tag{5b}$$

for some index m, where p is an arbitrary enumeration $p = 1, ..., M$ of all (k, l) and m such that $\text{int}(\overline{\Omega}^k \cap \overline{\Omega}^l)$ or $\text{int}(\overline{\Omega}^m \cap \partial\overline{\Omega})$ is not empty. The intersection of all closures of all γ^p defines a set of vertices $\mathcal{V}$ composed of all elements

$$v^q = \overline{\gamma}^m \cap \overline{\gamma}^n \tag{6}$$

where q is an arbitrary enumeration $q = 1, ..., V$ of all couples (m, n) for which $(\overline{\gamma}^m \cap \overline{\gamma}^n)$ is not

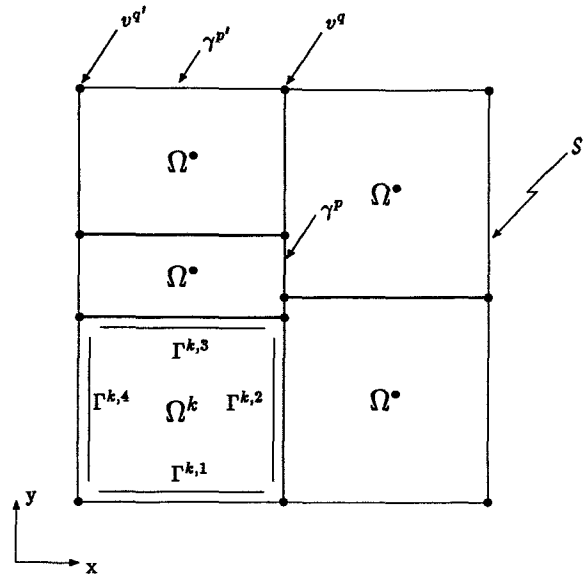

Figure 1: Subdomains and Mortars of a Nonconforming Decomposition

empty. (The set $\mathcal{V}$ is equal to the set of all the vertices of the Ω^k by definition of the mortars). Lastly, we define the skeleton S of the mortar system by

$$S = \bigcup_{p=1}^{M} \overline{\gamma}^p = \bigcup_{k=1}^{K} \partial\Omega^k. \tag{7}$$

The geometry of the nonconforming decomposition is shown graphically in Figure 1.

In order to define the nonconforming space X_h, we first require an auxiliary mortar space W_h

$$W_h = \{\phi \in C^0(S),\ \forall p = 1, ..., M,\ \phi_{|\gamma^p} \in \mathbf{P}_N(\gamma^p),\ \phi_{|\partial\Omega} = 0\} \tag{8}$$

where $\mathbf{P}_N(\gamma^p)$ is the space of all polynomials on γ^p of degree $\leq N$. The nonconforming space is then given by

$$X_h = \{v \in L^2(\Omega),\ \forall k = 1,...,K,\ v_{|\Omega^k} \in \mathbf{P}_N(\Omega^k) \text{ such that } \exists \phi \in W_h \text{ for which:}$$

$$\forall q = 1,...,V,\ \forall k = 1,...,K, \text{ such that } v^q \text{ is a vertex of } \Omega^k,\ v_{|\Omega^k}(v^q) = \phi(v^q); \quad (9a)$$

$$\text{and} \quad \forall l = 1,...,4,\ \forall k = 1,...,K,\ \forall \psi \in \mathbf{P}_{N-2}(\Gamma^{k,l}),\ \int_{\Gamma^{k,l}}(v_{|\Omega^k} - \phi)\psi ds = 0 \quad \}. \quad (9b)$$

Here $\mathbf{P}_N(\Omega^k)$ denotes the space of all polynomials on Ω^k of degree $\leq N$ in each spatial direction; the spectral element discretization parameter is the couple $h = (K, N)$. For a conforming approximation X_h is the standard spectral element space; here, and elsewhere in this paper, we assume the reader is familiar with the conforming spectral element method [22].

Let us summarize the properties of the approximation space X_h. First, as regards the uniqueness of the solution, we note that the uniqueness of the mortar element $\phi \in W_h$ is not of major importance as long as its image $u_h \in X_h$ is unique; it is u_h, not the mortar element, that must be close to u. The uniqueness of the discrete solution u_h follows from the ellipticity of the Laplacian form $(\nabla u_h, \nabla v_h)$, $\forall u_h \in X_h$, $\forall v_h \in X_h$ with respect to the following "broken $H^1(\Omega)$ norm",

$$\|v_h\|_{X_h} = \left[\sum_{k=1}^{K} \|(v_h)_{|\Omega^k}\|^2_{1,\Omega^k}\right]^{1/2}, \quad \forall v_h \in X_h. \quad (10)$$

Although the proof of ellipticity is quite involved (see [4]), an elementary proof of uniqueness can be readily derived. To wit, we note that if u_h and u'_h are two solutions of (4), we get

$$0 = (\nabla v_h, \nabla v_h) = \sum_{k=1}^{K} \int_{\Omega^k} [\nabla (v_h)_{|\Omega^k}]^2 \quad \text{with } v_h = u_h - u'_h,$$

and thus v_h is piecewise constant. Using the fact that the elements of X_h vanish over $\partial\Omega$ and are continuous at the vertices of $\mathcal{V}$, it follows that $v_h \equiv 0$ and thus $u_h = u'_h$.

Although uniqueness of $\phi \in W_h$ is not necessary, it is nevertheless true that spurious (or parasitic) modes in ϕ correspond to unprofitable work, and can potentially cause problems in the

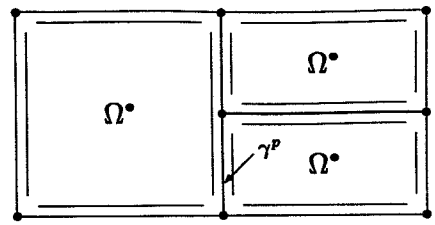

Figure 2: Nonconforming Discretization Derived from the Refinement of a Conforming Approximation

subsequent solution of the discrete system (see Section 3.2). There is one situation in which the uniqueness of ϕ follows easily; this is the case where for each γ^p there exists an element Ω^k that accepts γ^p as an entire edge (see Figure 2). This arises, for instance, from a refinement of a mesh which is initially conforming. In this paper we shall consider only this "refinement" case; development and analysis of the general problem of Figure 1 is more involved, and is relegated to future publications. For the "refinement" case uniqueness of ϕ results from the fact that the mortar element ϕ coincides exactly with the restriction $(v_h)_{|_{\Omega^k}}$ over γ^p. To show this we note that, by construction, the elements ϕ and $v_h^k = (v_h)_{|_{\Omega^k}}$ coincide at the endpoints of γ^p. This implies that $\phi - v_{h|_{\gamma^p}}^k$ is a polynomial of the local coordinate $\tilde{s}$,

$$(\phi - v_{h|_{\gamma^p}}^k)(\tilde{s}) = (1 - \tilde{s}^2)\Phi(\tilde{s}), \tag{11}$$

where Φ is a polynomial of degree $\leq N - 2$. Here, and in what follows, $\tilde{s} = \tilde{x}$ (or $\tilde{s} = \tilde{y}$) for a horizontal (or vertical) mortar, where $\tilde{x}$ (or $\tilde{y}$) is a mortar-local variable which scales x (or y) such that γ_p corresponds to $]-1,1[$ (similarly, $\hat{s} = \hat{x}$ (or $\hat{s} = \hat{y}$) for a horizontal (or vertical) edge, where $\hat{x}$ (or $\hat{y}$) is an element-local variable on $]-1,1[$ which scales x (or y) to the appropriate $\Gamma^{k,l}$). From

the orthogonality of $\phi - v^k_{h|\gamma^p}$ to all elements of $\mathbf{P}_{N-2}(\gamma^p)$ (9b), it follows that Φ is necessarily zero, and thus ϕ is exactly the trace of one piece of v_h. The uniqueness of the solution u_h to problem (4) thus yields the uniqueness of the corresponding mortar element.

Let us consider now the consistency error. The scheme (4) based on the definition (9a,9b) of X_h is optimal in that the consistency error is maintained small by the combination of the L^2 condition (9b) and the vertex condition (9a). In essence, the L^2 condition ensures that the jump in functions is small in the interior of internal boundaries, whereas the vertex condition ensures exact continuity at cross points where the normal derivative has more than one sense. We note that the superiority of the L^2- (versus pointwise-) matching of $v_{|_{\Omega^k}}$ and ϕ has been demonstrated previously [2]. The mortar methods are different from previously proposed nonconforming L^2 approximations in that the latter are mortarless master-slave spaces, whereas the current approach is democratic; this allows for very simple implementation in arbitrary topologies.

Lastly, the approximation properties of the space X_h are similar to those of past nonconforming approximations. For example, for the case of a square domain decomposed into several elements, as a first result one can use the best *global* polynomial approximation as a bound for approximation errors. The combination of stability, consistency and approximation result in an optimal scheme, the details, and degree of locality of which, are described in [4]. We note that for the special case of infinitely smooth solutions, u_h approaches u exponentially fast as $N \to \infty$ for fixed K (spectral convergence).

3 Representation and Discrete Equations

3.1 Bases

Although the spaces W_h and X_h appear quite complicated, they have a simple basis and evaluation procedure which yields an efficient domain decomposition algorithm. In this section we discuss the basis, and in the following section we describe residual evaluation.

To begin, we write for the space W_h,

$$\phi|_{\gamma^p} = \sum_{j=0}^{N} \phi_j^p h_j^N(\tilde{s}), \quad \forall p \in \{1, ..., M\} \tag{12}$$

where we assume that all indices increase with increasing x, y. Here the h_j^N are Lagrangian interpolants defined by

$$h_j^N \in \mathbf{P}_N(]-1,1[), \quad h_j^N(\xi_i) = \delta_{ij}, \quad \forall i,j \in \{0, ..., N\}^2 \tag{13}$$

where the $\xi_i (= \xi_i^N)$ are the $N+1$ Gauss-Lobatto Legendre points defined by the zeroes of $L_N'(z)(1-z^2)$, and L_N is the Legendre polynomial of order N [30] so that

$$h_j^N(z) = -\frac{1}{N(N+1)L_N(\xi_i)} \frac{(1-z^2)L_N'(z)}{z-\xi_i} \quad z \in]-1,1[, \quad \forall j \in \{0, ..., N\}.$$

The definition (12) is not sufficient given the requirement that $\phi \in W_h$ must be $C^0(S)$; to indicate the continuity condition, we resort to diagrammatic methods. The mortar conventions are described in Table 1a, with the basis for W_h shown in Figure 3b for the nonconforming mesh of Figure 3a.

We next construct a representation for $v \in X_h$ in terms of the mortar. To begin, we write

$$v|_{\Omega^k} = \sum_{i=0}^{N} \sum_{j=0}^{N} v_{ij}^k h_i^N(\hat{x}) h_j^N(\hat{y}), \quad \forall k \in \{1, ..., K\} \tag{14}$$

where the h_i^N are defined in (13). The internal degrees-of-freedom, v_{ij}^k, $i,j \in \{1, ..., N-1\}^2$, are clearly free, however the boundary degrees-of-freedom are constrained through (9a,9b). Based on

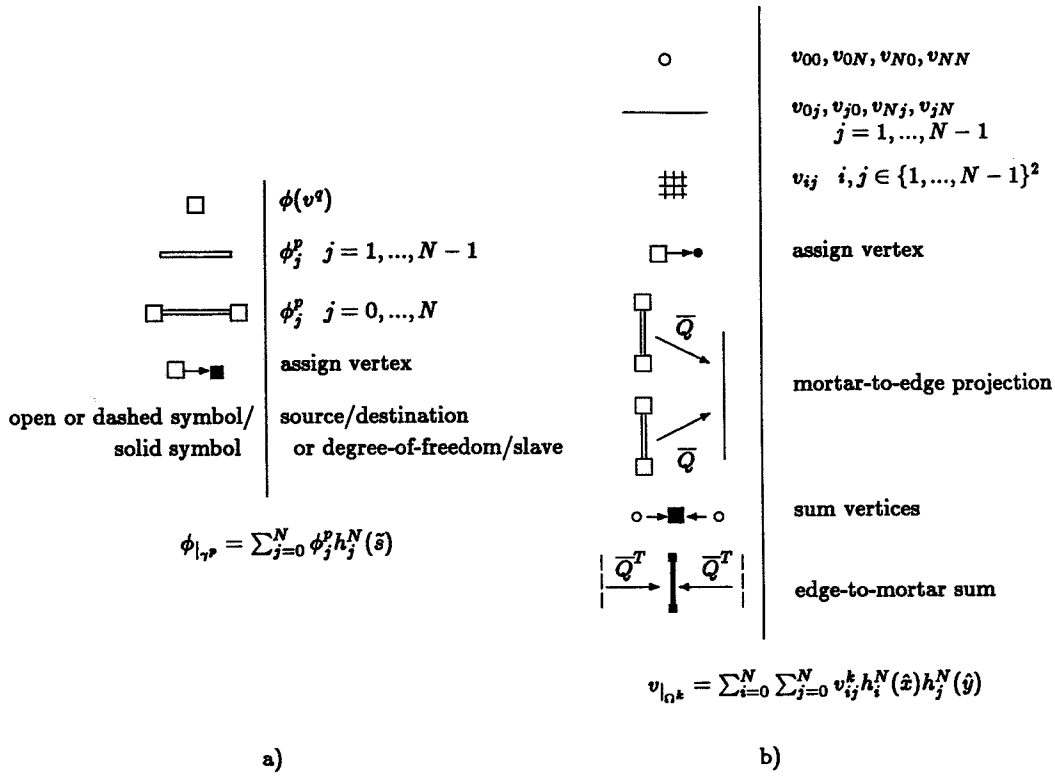

Table 1: Symbols for Diagrammatic Basis Representation

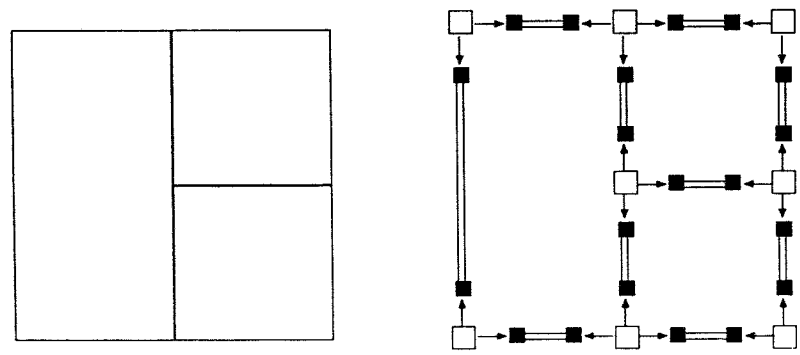

Figure 3: a) Nonconforming Mesh and b) Associated Mortar Basis

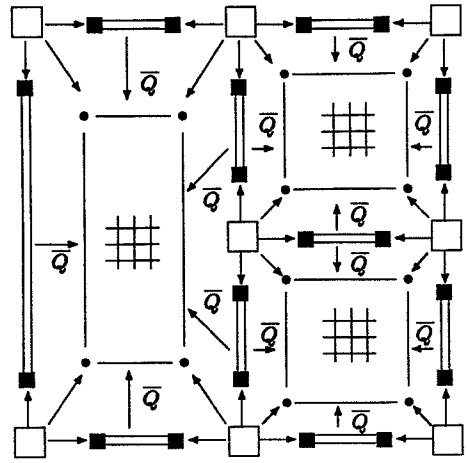

Figure 4: Diagrammatic Representation of the Basis for X_h on Nonconforming Mesh of Fig. 3a

the diagrammatic conventions of Table 1 the admissible v are given by Figure 4, where $\overline{Q}$ derives from the projection (9b). In order to construct $\overline{Q}$ we require a basis for ψ, which we choose as

$$\psi_{|_{\Gamma^{k,l}}} = \sum_{q=1}^{N-1} \beta_q \eta_q^{N-2}(\hat{s}) \tag{15}$$

where

$$\eta_q^{N-2}(z) = (-1)^{N-q} \frac{L_N'(z)}{\xi_q - z} \quad z \in]-1,1[, \quad q \in \{1,...,N-1\}. \tag{16}$$

To calculate the projection of (9b) we then perform (here exact) piecewise Gauss-Lobatto quadrature on $N+1$ points on the element edges and mortar segments, giving

$$\sum_{j=1}^{N-1} \overline{B}_{ij} v_j = \sum_{j=0}^{N} \overline{P}_{ij} \phi_j, \quad \forall i \in \{1,...,N-1\} \tag{17}$$

where for the destination edge $\Gamma^{k,l}$ (v_j) and source mortar γ^p (ϕ_j)

$$\int_{\Gamma^{k,l}} v\psi \longrightarrow \overline{B}_{ij} = \frac{|\Gamma^{k,l}|}{2}(-1)^{N-i}(-L_N''(\xi_i))\rho_i \delta_{ij}, \quad \forall i,j \in \{1,...,N-1\}^2 \tag{18}$$

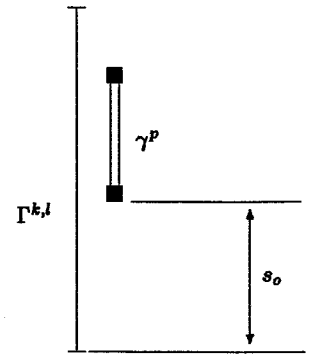

Figure 5: Definition of Mortar Offset s_o

and

$$\int_{\Gamma^{k,l}} \phi_{|\gamma^p} \psi \longrightarrow \overline{P}_{ij} = \frac{|\gamma^p|}{2} \eta_i^{N-2} \left(2\frac{s_o}{|\Gamma^{k,l}|} - 1 + (\xi_j + 1)\frac{|\gamma^p|}{|\Gamma^{k,l}|}\right)\rho_j - \begin{cases} \frac{|\Gamma^{k,l}|}{2}\eta_i^{N-2}(-1)\rho_0\delta_{0,j} & \text{if } s_o = 0 \\ \frac{|\Gamma^{k,l}|}{2}\eta_i^{N-2}(1)\rho_N\delta_{N,j} & \text{if } s_o + |\gamma^p| = |\Gamma^{k,l}| \end{cases} \quad \forall i \in \{1,...,N-1\} \ \forall j \in \{0,...,N\}. \tag{19}$$

Here s_o is the offset of the mortar γ^p from the edge $\Gamma^{k,l}$, as shown in Figure 5; the endpoint terms of (19) derive from the vertex-pinning condition of (9a). Finally we arrive at

$$\overline{Q}_{ij} = [\overline{Q}] = [\overline{B}]^{-1}[\overline{P}], \quad \forall i \in \{1,...,N-1\}, \ \forall j \in \{0,...,N\}. \tag{20}$$

Note that by proper choice of the basis for ψ we can explicitly form the matrix $\overline{Q}$, that is, we are able to directly invert the diagonal inner product $\overline{B}$. The alternating-sign term in η_q^{N-2} assures that the entries of $\overline{B}$ are positive.

Although in practice we shall evaluate $v_{|_{\Omega^k}}$ from the diagram without forming the global linear projection operator, it is nevertheless of theoretical interest to remark that the diagram is equivalent to

$$\begin{pmatrix} v^k_{ij}|_{interior},\ \forall k \\ v^k_{ij}|_{interface},\ \forall k \end{pmatrix} = \begin{pmatrix} [I] & 0 \\ 0 & [\overline{Q}] \end{pmatrix} \begin{pmatrix} v^k_{ij}|_{interior},\ \forall k \\ \phi(v^q),\ \forall q,\ \phi^p_j,\ \forall p,\ \forall j \in \{1,...,N-1\} \end{pmatrix} \tag{21a}$$

or

$$\underline{v}^* = Q\underline{v}. \tag{21b}$$

We denote the vector $\underline{v}$ as the *algebraic* basis, in that this variable represents the finite-dimensional approximation space with an equivalent number of degrees-of-freedom; the proper *functional* basis corresponds to the images of $\underline{v}^T = (1,0,0...),(0,1,0,....),...,(0,...,0,1)$ in $\underline{v}^*$ through the transformation Q, acting on the local bases h_ih_j as described by (14).

3.2 Discrete Equations

Armed with the variational forms of Section 2 and the bases of Section 3.1, it is now a simple matter to construct the discrete equations. In particular, we note that our basis construction (21) allows us to express admissible elemental degrees-of-freedom $\underline{v}^*$ in terms of $\underline{v}$. This, in turn, permits us to construct the global discrete equations directly from local structure-preserving elemental equations, which is at the heart of the discretization-driven domain decomposition approach.

We first construct the decoupled elemental matrices and inhomogeneity,

$$blk(\hat{A}^k) = \begin{pmatrix} (\nabla h_ph_q, \nabla h_ih_j)^{k=1} & 0 & 0 \\ 0 & (\nabla h_ph_q, \nabla h_ih_j)^{k=2} & 0 \\ & & \\ 0 & 0 & (\nabla h_ph_q, \nabla h_ih_j)^{k=K} \end{pmatrix} \tag{22}$$

$$blk(\hat{f}^k) = \begin{pmatrix} (h_p h_q, f)^{k=1} \\ (h_p h_q, f)^{k=2} \\ \\ \\ \cdot \\ \\ (h_p h_q, f)^{k=K} \end{pmatrix}, \qquad \forall i,j,p,q \in \{0,...,N\}^4.$$

The kth block of $blk(\hat{A}^k)$ represents the Neumann Laplace operator on the elemental domain Ω^k. We now recognize that not all elemental $h_i h_j$ are possible, and that not all $h_p h_q$ are admissible; indeed, the admissible degrees-of-freedom follow from the Q transformation of (21). We thus arrive, rather simply, at the fully discrete equations:

$$Q^T blk(\hat{A}^k) Q \underline{u} = Q^T blk(\hat{f}^k). \tag{23}$$

We note that independent of the size of the mortar nullspace (Q right nullspace), (23) is solvable. A sufficient condition for a unique mortar function is that $Q^T Q$ be invertible; in the conforming cases $Q^T Q$ is simply the multiplicity of a node (that is, the number of elements in which it appears).

Equation (23) illustrates that the global Laplace operator can be thought of as a local operator "mortared" together by the Q^T, Q operations; indeed, the Q^T operator is the algebraic form of the standard direct stiffness procedure (here extended to nonconforming elements). In the implementation of iterative procedures the Q, Q^T are, of course, never explicitly formed, but rather are evaluated; diagrammatic evaluation of Q^T (direct stiffness summation) is shown in Figure 6 in terms of the diagram conventions defined in Table 1. The domain decomposition decoupling afforded by the implicit construction of the image basis through $\underline{u}^*$ allows for efficient parallel implementation following the methods described in [11] for conforming techniques.

Although the emphasis in the current paper is on the mortar discretization, the bases and

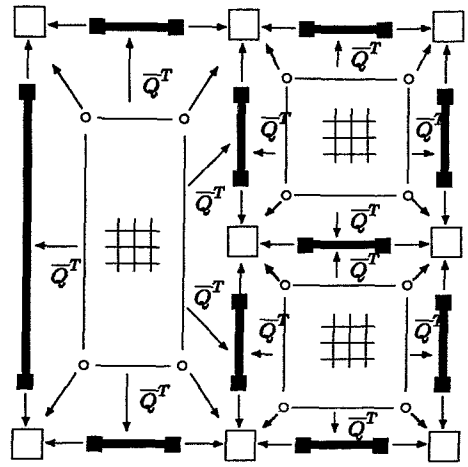

Figure 6: Direct Stiffness Summation Q^T of Residuals on Nonconforming Mesh

evaluation procedure have been tailored to admit efficient iterative solution, and it is therefore appropriate to briefly indicate how the method is used in conjunction with (for example) conjugate gradient iteration. To solve (23) we write

$$\underline{u}_0; \qquad \underline{r}_0 = Q^T blk(\hat{f}^k) - Q^T blk(\hat{A}^k) Q \underline{u}_0; \qquad \underline{q}_0 = \underline{r}_0 \tag{24}$$

$$a_m = (\underline{r}_m, \underline{r}_m)/(\underline{q}_m, Q^T blk(\hat{A}^k) Q \underline{q}_m)$$

$$\underline{u}_{m+1} = \underline{u}_m + a_m \underline{q}_m$$

$$\underline{r}_{m+1} = \underline{r}_m - a_m Q^T blk(\hat{A}^k) Q \underline{q}_m$$

$$b_m = (\underline{r}_{m+1}, \underline{r}_{m+1})/(\underline{r}_m, \underline{r}_m)$$

$$\underline{q}_{m+1} = \underline{r}_{m+1} + b_m \underline{q}_m,$$

where m refers to iteration number, $\underline{r}_m$ is the residual, $\underline{q}_m$ the search direction and $(.,.)$ is the usual discrete inner product. All evaluations are performed through the diagrams of Figures 4 and 6. The $blk(\hat{A}^k)$ operations are entirely local at the elemental level, with all transmission and

coupling through Q. The local $\hat{A}^k$ calculations are the standard conforming spectral element tensor product evaluations, as the mortar decoupling allows all local structure to remain intact despite global irregularity (e.g. non-propagating mesh refinement).

4 The Stokes and Navier-Stokes Problems

In this section we consider the extension of the nonconforming mortar method to the solution of the two-dimensional steady Stokes problem in a rectangularly-decomposable domain Ω,

$$\begin{aligned} -\nu\nabla^2\mathbf{u} - \nabla p &= \mathbf{f} \\ \mathrm{div}\mathbf{u} &= 0, \end{aligned} \tag{25}$$

with homogeneous Dirichlet velocity boundary conditions $\mathbf{u} = 0$ on $\partial\Omega$. Here $\mathbf{u}$ is the velocity, p is the pressure, $\mathbf{f}$ is the forcing vector, and ν is the kinematic viscosity. The associated variational problem is: Find $(\mathbf{u}, p) \in (H_o^1(\Omega)^2, L_o^2(\Omega))$ such that

$$\begin{aligned} \nu(\nabla\mathbf{u}, \nabla\mathbf{w}) - (p,\ \mathrm{div}\mathbf{w}) &= (\mathbf{f}, \mathbf{w}), \quad \forall \mathbf{w} \in H_o^1(\Omega)^2 \\ (q, \mathrm{div}\ \mathbf{u}) &= 0, \quad \forall q \in L_o^2(\Omega), \end{aligned} \tag{26}$$

where $L_o^2(\Omega)$ is the space of L^2 functions of zero mean.

The discrete formulation of the problem consists of choosing two discrete approximation spaces, one for the velocity field and one for the pressure. It is shown in [3,22,24] for the conforming spectral element approximation that choosing *both* of these spaces to be polynomials of degree less than or equal to the *same* degree N leads to an ill-posed problem, in which spurious pressure modes arise [5,12]. The existence of such modes is in contradiction with the verification of the "inf-sup" condition [5]. As regards our nonconforming methods for the Stokes problem, our starting

point is the conforming staggered mesh method defined in [23] for which the "inf-sup" condition is satisfied. The correct nonconforming extension is to use the velocity space $(X_h)^2$ defined in (9a,9b), and for the pressure the space $M_h = \{\phi \in L^2,\ \phi_{|_{\Omega^k}} \in \mathbf{P}_{N-2}(\Omega^k)\}$ associated with the conforming approximation. In essence, the fact the pressure is L^2 implies that it need not be modified when the constraints on the velocity are relaxed.

With these spaces we arrive at the following nonconforming discretization:

Find $(\mathbf{u}_h, p_h) \in ((X_h)^2, M_h)$ such that

$$\begin{aligned} \nu(\nabla \mathbf{u_h}, \nabla \mathbf{w_h}) - (p_h,\ \mathrm{div}\mathbf{w_h}) &= < \mathbf{f}, \mathbf{w_h} >, \quad \forall \mathbf{w_h} \in (X_h)^2 \\ (q_h, \mathrm{div}\ \mathbf{u_h}) &= 0, \quad \forall q_h \in M_h \end{aligned} \tag{27}$$

from which uniqueness, stability, and spectral error properties follow from the results of previous sections and [4], suitably modified within the Stokes context as described in [23,24]. (We note that, as elsewhere in this paper, we do not dwell on quadrature issues which are, by now, standard practice.) We then choose a basis for M_h

$$p_{|_{\Omega^k}} = \sum_{i=1}^{N-1}\sum_{j=1}^{N-1} p_{ij}^k g_i^{N-2}(\hat{x}) g_j^{N-2}(\hat{y}), \quad \forall k \in \{1, ..., K\} \tag{28}$$

where the g_j^{N-2} are the $N-2$th order Gauss-Legendre interpolants, that is, those polynomials of $\mathbf{P}_{N-2}$ such that $g_j^{N-2}(\zeta_i^{N-2}) = \delta_{ij}$, where ζ_i^{N-2} are the $N-2$ zeroes of L_{N-2} [30]. We thus arrive at the discrete saddle problem

$$\begin{aligned} Q^T blk(\hat{A}^k) Q\underline{\mathbf{u}} - Q^T blk(\hat{\mathbf{D}}^k)^T \underline{p} &= Q^T blk(\hat{\mathbf{f}}^k) \\ blk(\hat{\mathbf{D}}^k) Q\underline{\mathbf{u}} &= 0. \end{aligned} \tag{29}$$

Here $\underline{p}$ is the algebraic basis for p analogous to $\underline{\mathbf{u}}$ of (21b), $blk(\hat{A}^k), Q^T, Q, blk(\hat{\mathbf{f}}^k)$ are defined as in

(18-22), and $\hat{\mathbf{D}}$ is the gradient operator given by

$$blk(\hat{\mathbf{D}}^k) = \begin{pmatrix} (g_p^{N-2} g_q^{N-2}, \nabla h_i h_j)^{k=1} & 0 & \cdot & 0 \\ 0 & (g_p^{N-2} g_q^{N-2}, \nabla h_i h_j)^{k=2} & & 0 \\ & \cdot & & \\ & & \cdot & \\ 0 & 0 & & (g_p^{N-2} g_q^{N-2}, \nabla h_i h_j)^{k=K} \end{pmatrix} \tag{30}$$

$$\forall i, j \in \{0, ..., N\}^2, \quad \forall p, q \in \{1, ..., N-1\}^2.$$

Extension to Navier-Stokes is straightforward given the lower-order nature of the convective terms.

As in the pure elliptic discretization, (29) is amenable to iterative solution. We currently use a semi-implicit procedure for Navier-Stokes, in which the nonlinear terms are treated explicitly, and the Stokes subproblem is handled with a Uzawa nested iteration [20]; conforming multigrid techniques [28] are currently being extended to the nonconforming case. In addition to the staggered mesh Stokes treatment, elliptic-splitting methods appropriate for higher Reynolds number flows are also used [17,19]; these discretizations represent sequences of elliptic operations (23), and thus their extension to the nonconforming case follows from Sections 2 and 3.

5 Numerical Examples

In this section we illustrate various aspects of our nonconforming method by a number of examples. The central point is the flexibility and ease-of-implementation afforded by a nonconforming approach based on a consistent, non-context-dependent matching. As our first example we consider

the Helmholtz problem

$$-\nabla^2 u + \lambda^2 u = f \quad \text{on} \quad \Omega =]0,1[\times]0,1[\tag{31}$$

$$u = e^{\frac{\lambda}{\sqrt{2}}((x-1)+(y-1))} \quad \text{on} \quad \partial\Omega$$

where f is chosen such that the exact solution in Ω is given by $u = e^{\frac{\lambda}{\sqrt{2}}((x-1)+(y-1))}$. In Figure 7a we show a high-resolution conforming mesh $h = (K = 16, N = \bullet)$; in Figure 7b we show a nonconforming mesh $h = (K = 10, N = \bullet)$, in which the local structure-preserving mesh refinement is illustrated. In Figure 8 we plot the error in the X_h norm of (10) for both solutions as a function of N (K fixed) for $\lambda = 50$. This example demonstrates the rapid (here exponential) convergence of the spectral element approach, and the superior resolution properties of the nonconforming discretization, which achieves the same accuracy as the conforming approximation with significantly fewer degrees-of-freedom.

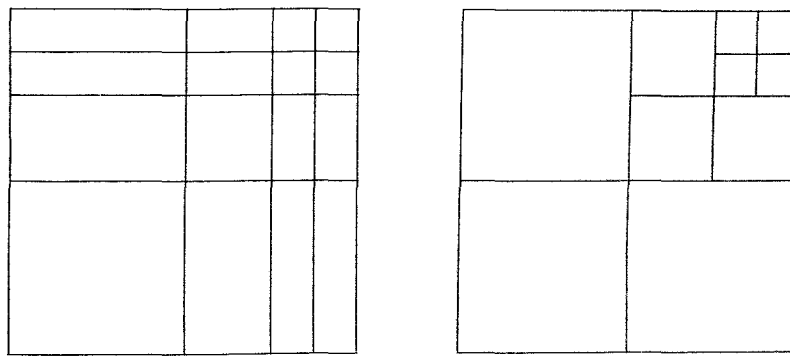

Figure 7: High Resolution a) Conforming and b) Nonconforming Meshes for Helmholtz Problem

As our second example we demonstrate the utility of nonconforming methods in constructing appropriate meshes; we consider the labyrinth channel of Figure 9, in which the two meshes for the

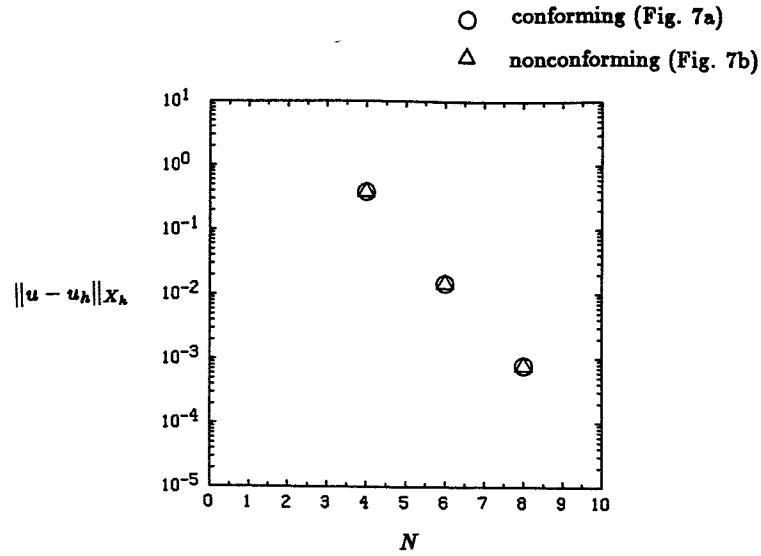

Figure 8: Convergence of the Broken H^1 Error for Helmholtz Problem

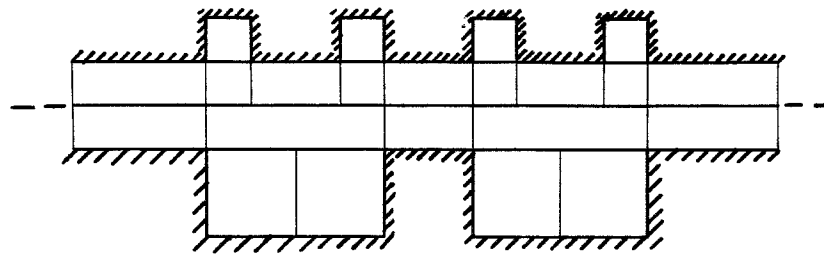

Figure 9: Nonconforming Labyrinth Channel Mesh, $h = (K = 22, N = 9)$

two sides of the channel are constructed "separately", and subsequently merged by mortar. The boundary conditions are given as: a parabolic velocity profile at inflow, no slip on the channel walls, and outflow (constant pressure) at the exit. In Figure 10 we show streamlines for the steady Stokes flow calculated by the discretization (29) and the nested conjugate gradient Uzawa method; notable are the continuity at element boundaries and the lack of spurious pressure modes. The mesh in Figure 9 can be thought of as one instance of a sliding channel calculation; nonconforming methods, with appropriate extension (as in Figure 1), should prove to be powerful techniques for moving boundary problems when used in conjunction with arbitrary-Lagrangian-Eulerian techniques [15].

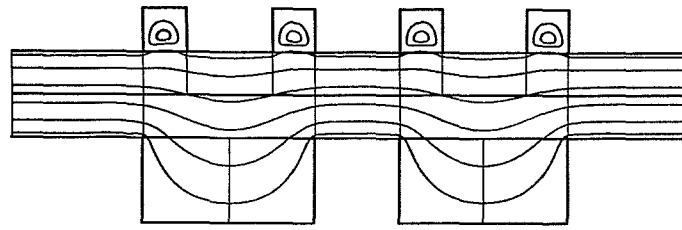

Figure 10: Stokes Solution for the Labyrinth Channel

Lastly, we consider a moderate Reynolds number flow past a wedge [17,26] in a channel; the utility of the nonconforming methods in generating an appropriately refined mesh is apparent in the mesh shown in Figure 11. Note that we relax here the constraint, introduced for simplicity of exposition in previous sections, that the elements be rectangular; treatment of general curved elements represents a simple extension of the methods described in Sections 2-4. In Figure 12 we show the short time solution of the startup vortex near the tip of the wedge, for a Reynolds number $R = 500$ at a time $\tau = \frac{tV}{H} = .085$ on the mesh $h = (K = 16, N = 9)$ of Figure 11. We prescribe a slug velocity profile at inflow, no slip boundary conditions on the walls, and outflow (constant pressure) at the exit. Here $R = \frac{VH}{\nu}$, where V is the channel average velocity, H the channel width, and ν is the kinematic viscosity, and t is time. The high resolution in the vicinity of the wedge allows for a detailed description of the startup vortex.

Acknowledgements

This work was supported by Avions Marcel Dassault-Bréguet Aviation, the ONR and DARPA under Contract N00014-85-K-0208, the ONR under Contract N00014-88-K-0188, and the NSF under Grant ASC-8806925. This work was partially done while the first author was in residence at ICASE.

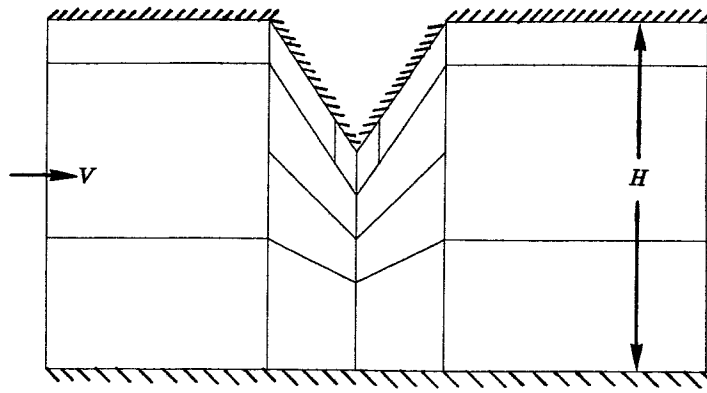

Figure 11: Nonconforming Mesh for Startup Flow Past a Wedge

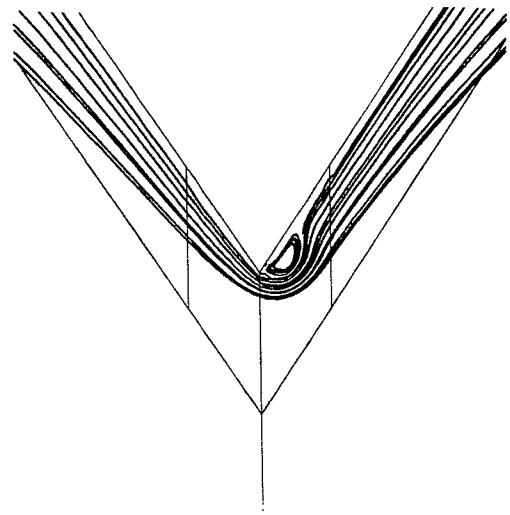

Figure 12: Navier-Stokes Solution for Flow Past a Wedge at $R = 500$, $r = .085$

References

[1] R. Adams. *Sobolev Spaces.* Academic Press, 1975.

[2] C. Bernardi, N. Débit, and Y. Maday. Coupling spectral and finite element methods for the Laplace equation. *Mathematics of Computation,* to appear (also ICASE report no. 87-70 and Publication du Laboratoire d'Analyse Numérique de l'Université Pierre et Marie Curie, no. 87031).

[3] C. Bernardi, Y. Maday, and B. Métivet. Calcul de la pression dans la résolution spectrale du problème de Stokes or Computation of the pressure in the spectral approximation of the Stokes problem. *La Recherche Aérospatiale (and English edition),* 1–21, 1987.

[4] C. Bernardi, Y. Maday, and A.T. Patera. A new nonconforming approach to domain decomposition: the mortar element method. In H. Brezis and J. L. Lions, editors, *Nonlinear Partial Differential Equations and Their Applications, Collège de France Seminar,* Pitman, to appear.

[5] F. Brezzi. On the existence, uniqueness and approximation of saddle-point problems arising from Lagrange multipliers. *Rairo Anal. Numer.,* 8 R(2), 129, 1974.

[6] C. Canuto, M. Y. Hussaini, A. Quarteroni, and T. A. Zang. *Spectral Methods in Fluid Dynamics.* Springer-Verlag, 1987.

[7] T. Chan, editor. *Proceedings of the Second International Conference on Domain Decomposition Methods for Partial Differential Equations,* SIAM, Philadelphia, 1988.

[8] P. Ciarlet. *The Finite Element Method.* North Holland, 1978.

[9] M. Dorr. Domain decomposition via Lagrange multipliers. *submitted to Numerische Mathematik*, 1988.

[10] P. F. Fischer, L. W. Ho, G. E. Karniadakis, E. M. Rønquist, and A. T. Patera. Recent advances in parallel spectral element simulation of unsteady incompressible flows. *Proceedings of the Symposium on Advances and Trends in Computational Structural Mechanics and Computational Fluid Dynamics, Washington, D.C.*, 1988.

[11] P. F. Fischer and A. T. Patera. Parallel spectral element solution of the Stokes problem. *submitted to Journal of Computational Physics*, 1988.

[12] V. Girault and P. A. Raviart. *Finite Element Methods for the Navier-Stokes Equations.* Springer, 1986.

[13] R. Glowinski, G. Golub, G. Meurant, and J. Périaux, editors. *Proceedings of the First International Conference on Domain Decomposition Methods for Partial Differential Equations*, SIAM, Philadelphia, 1987.

[14] D. O. Gottlieb and S.A. Orszag. *Numerical Analysis of Spectral Methods.* SIAM, Philadelphia, 1977.

[15] L. W. Ho. *A Spectral Element Method for Free-Surface and Moving Boundary Flows.* PhD thesis, Massachusetts Institute of Technology, 1989.

[16] G. E. Karniadakis. Numerical simulation of heat transfer from a cylinder in crossflow. *International Journal of Heat and Mass Transfer*, **31**(1), 107, 1988.

[17] G. E. Karniadakis. Spectral element simulations of laminar and turbulent flows in complex geometries. *Numerical Applied Mathematics*, to appear, 1988.

[18] G. E. Karniadakis, B. B. Mikic, and A. T. Patera. Minimum-dissipation transport enhancement by flow destabilization: Reynolds' analogy revisited. *Journal of Fluid Mechanics*, **192**, 365, 1988.

[19] K.Z. Korczak and A.T. Patera. An isoparametric spectral element method for solution of the Navier-Stokes equations in complex geometry. *Journal of Computational Physics*, **62**, 361, 1986.

[20] Y. Maday, D.I. Meiron, A.T. Patera, and E.M. Rønquist. Iterative saddle problem decomposition methods for the steady and unsteady Stokes equations. *submitted to Journal Computational Physics*, 1988.

[21] Y. Maday and R. Muñoz. Spectral element multigrid. II. theoretical justification. *submitted to Journal of Scientific Computing*, 1988.

[22] Y. Maday and A.T. Patera. Spectral element methods for the Navier-Stokes equations. In A.K. Noor, editor, *State-of-the-art surveys in computational mechanics*, ASME, New York, 1988.

[23] Y. Maday, A.T. Patera, and E.M. Rønquist. The $\mathbf{P}_n - \mathbf{P}_{N-2}$ Legendre spectral element method for the multi-dimensional Stokes problem. in preparation.

[24] Y. Maday, A.T. Patera, and E.M. Rønquist. Optimal Legendre spectral element methods for the Stokes semi-periodic problem. *submitted to SIAM Journal of Numerical Analysis*.

[25] A.T. Patera. A spectral element method for fluid dynamics: laminar flow in a channel expansion. *Journal of Computational Physics*, **54**, 468, 1984.

[26] D. I. Pullin and A. E. Perry. Some flow visualization experiments on the starting vortex. *Journal of Fluid Mechanics*, **97**, 239, 1980.

[27] E. M. Rønquist. *Optimal Spectral Element Methods for the Unsteady Three-Dimensional Incompressible Navier-Stokes Equations.* PhD thesis, Massachusetts Institute of Technology, 1988.

[28] E.M. Rønquist and A.T. Patera. Spectral element multigrid. I. Formulation and numerical results. *Journal of Scientific Computing*, **2**(4), 389, 1987.

[29] G. Strang and G. Fix. *An Analysis of the Finite Element Method.* Prentice-Hall, 1973.

[30] A.H. Stroud and D. Secrest. *Gaussian Quadrature Formulas.* Prentice Hall, Englewood Cliffs, New Jersey, 1966.

[31] J. M. Thomas. *Sur l'analyse numérique des méthodes d'éléments finis hybrides et mixtes.* Thèse d'Etat, Université Pierre et Marie Curie, 1987.

[32] T.A. Zang, Y.S. Wong, and M.Y. Hussaini. Spectral multigrid methods for elliptic equations. *Journal of Computational Physics*, **48**, 485, 1982.